

Letters to *Analytical Chemistry*

Spatial Correlation of Confocal Raman Scattering and Secondary Ion Mass Spectrometric Molecular Images of Lignocellulosic Materials

Zhen Li,^{†,‡} Li-Qiang Chu,[§] Jonathan V. Sweedler,[†] and Paul W. Bohn^{*,§}

Department of Chemical and Biomolecular Engineering and Department of Chemistry and Biochemistry, University of Notre Dame, Notre Dame, Indiana 46556, and Department of Chemistry, Beckman Institute and Institute for Genomic Biology, University of Illinois at Urbana–Champaign, Urbana, Illinois 61801

A detailed chemical and structural understanding of pre-enzymatic processing of lignocellulosic materials (LCMs) is a key objective in the development of renewable energy. Efficient rendering of biomass components into fermentable substrates for conversion into biofuel feedstocks would benefit greatly from the development of new technologies to provide high-quality, spatially resolved chemical information about LCMs during the various processing states. In an effort to realize this important goal, spatially correlated confocal Raman and mass spectrometric images allow the extraction of three-dimensional information from the perennial grass, *Miscanthus x giganteus*. An optical microscopy-based landmark registry scheme was developed that allows samples to be transferred between laboratories at different institutions, while retaining the capability to access the same physical regions of the samples. Subsequent to higher resolution imaging via confocal Raman microscopy and secondary ion mass spectrometry (SIMS), laser desorption-ionization mass spectrometry was used to place these regions within the overall sample architecture. Excellent sample registry was evident in the highly correlated Raman and SIMS images. In addition, the correlation of vibrational Raman scattering with mass spectra from specific spatial locations allowed confirmation of the assignment of intracellular globular structures to hemicellulose-rich lignin complexes, an assignment which could only be made tentatively from either image alone.

Lignocellulosic materials (LCMs), such as switchgrass, *Miscanthus*, and corn/wheat stalks, have attracted considerable interest because of their potential as feedstocks for biofuel

production.^{1,2} It is well-known that LCMs are heterogeneous composites, with complex cell walls consisting principally of cellulose, hemicelluloses, and lignin. The conversion of LCMs into biofuels typically involves three steps: (1) pretreatment, which allows for the separation of cellulose and/or hemicelluloses from lignin; (2) saccharification or the enzymatic hydrolysis of cellulose/hemicellulose into monomeric sugars; and (3) fermentation, which converts sugars into ethanol using yeast. The first step, pretreatment, is critical, since saccharification cannot proceed in the presence of a significant amount of lignin. Thus, a great deal of effort is being put into the optimization of pretreatment processes in order to reduce total LCM biorefining costs.^{3–5} Efficient pretreatment can improve the enzymatic hydrolysis of cellulose by disrupting the cell wall structure, reducing the crystallinity of cellulose, and increasing the accessible area. Nearly all studies of pretreatment protocols have had to rely on composite evaluative data, such as cellulose yield, to guide development. Clearly, the ability to directly visualize the molecular nature of LCMs as a function of pretreatment protocols would be enormously beneficial.^{6–8} To this end, spatially correlated Raman scattering and secondary ion mass spectrometry (SIMS) imaging have been combined here to assess *Miscanthus x giganteus* from the same samples at the same locations.

Specifically, confocal Raman microscopy (CRM) and SIMS imaging were used to correlate optical and mass spectrometric data and generate chemical information as a function of spatial position and processing time. CRM has proved to be a sensitive

- (1) Ragauskas, A. J.; Williams, C. K.; Davison, B. H.; Britovsek, G.; Cairney, J.; Eckert, C. A.; Frederick, W. J.; Hallett, J. P.; Leak, D. J.; Liotta, C. L.; Mielenz, J. R.; Murphy, R.; Templer, R.; Tschaplinski, T. *Science* **2006**, *311*, 484–489.
- (2) Tilman, D.; Hill, J.; Lehman, C. *Science* **2006**, *314*, 1598–1600.
- (3) Hendriks, A.; Zeeman, G. *Bioresour. Technol.* **2009**, *100*, 10–18.
- (4) Kumar, P.; Barrett, D. M.; Delwiche, M. J.; Stroeve, P. *Ind. Eng. Chem. Res.* **2009**, *48*, 3713–3729.
- (5) Mosier, N.; Wyman, C.; Dale, B.; Elander, R.; Lee, Y. Y.; Holtapple, M.; Ladisch, M. *Bioresour. Technol.* **2005**, *96*, 673–686.
- (6) Singh, S.; Simmons, B. A.; Vogel, K. P. *Biotechnol. Bioeng.* **2009**, *104*, 68–75.
- (7) Orts, W. J.; Holtzman, K. M.; Seiber, J. N. *J. Agric. Food Chem.* **2008**, *56*, 3892–3899.
- (8) McCann, M. C.; Carpita, N. C. *Curr. Opin. Plant Biol.* **2008**, *11*, 314–320.

* To whom correspondence should be addressed. Phone: (+1) 574 6311849. Fax: (+1) 574 6318366. E-mail: pbohn@nd.edu.

† University of Illinois at Urbana–Champaign.

‡ Current address: Materials Characterization Facility (MCF), Texas A&M University, College Station, TX 77843.

§ University of Notre Dame.

and nondestructive technique for plant study, as exemplified by the investigation of cellulose and woody tissues *in situ*.^{9–12} Raman scattering is not sensitive to water interference nor does it require complex sample preparation, making it particularly suitable for *in situ* observation of biological samples. Even in complex matrixes where spatial resolution is degraded, lateral resolution, $\Delta x = (0.61\lambda)/NA$, as determined by the laser wavelength, λ , and the numerical aperture, NA, of the objective,^{13–15} can approach $\sim 1 \mu\text{m}$. SIMS imaging has also been widely employed to investigate tissue sections and single cells because direct analysis of the tissue composition can be achieved without labeling, and multiple species can be detected simultaneously.^{16–19} The diameter of the primary ion beam can be $<200 \text{ nm}$, allowing for the visualization of tissue sections with submicrometer resolution. The spatial resolution achieved with SIMS is comparable to that of CRM, and the two imaging methods yield complementary chemical information. Laser desorption ionization mass spectrometry (LDI-MS), achieved by rastering the focused laser across the sample and correlating detected ions with the location of the focal spot, has been used to visualize the distribution of various compounds, especially proteins and peptides, in tissue sections and in single cells.^{17,20–23} The laser spot-size, typically $\sim 50 \mu\text{m}$, limits the spatial resolution; however, the potential to observe high-mass species makes LDI-MS a valuable complement to SIMS and CRM. Both SIMS and LDI instrumentation and protocols have been adapted to characterizing a range of compounds found within plant tissues.^{24–29}

Previous efforts to obtain correlated CRM and SIMS examined drug-coated stainless steel stents and coupons; however, because of the requirements of sample preparation, the images were not

obtained from the same sample nor at the same location.³⁰ Correlated CRM and SIMS analyses on the same sample at the same location was successfully accomplished in supracrustal rocks;³¹ however, the dynamic SIMS used in that case yielded mostly atomic secondary ions. Other vibrational-based microscopy methods have been coupled with SIMS for the imaging of biological samples,³² but there are no reports of correlating CRM with static SIMS images to our knowledge.

Here, CRM and SIMS are combined with LDI-MS to investigate the structural and chemical information in a model LCM, *Miscanthus x giganteus*, a tall perennial grass and potential energy crop for conversion to either fuel or chemicals. The approach used to correlate spatial positions among the three different imaging modalities is shown in Figure S1 and detailed in the Supporting Information. Briefly, the irregular shape of the *Miscanthus* samples can be imaged optically and used to provide an *in situ* map, with readily identifiable landmarks that serve as registration aids when transferring samples between laboratories. Figure S1 in the Supporting Information shows that the LDI mass spectra were acquired from a grid of points, these data being obtained after high-resolution imaging by CRM and SIMS to allow larger areas to be probed for higher molecular weight compounds.

Figure 1 outlines the overall strategy. First, CRM imaging was used to analyze the *Miscanthus* cross sections in an ambient environment. Characteristic bands of cellulose ($345\text{--}390 \text{ cm}^{-1}$) and lignin ($1550\text{--}1650 \text{ cm}^{-1}$) were monitored. The CRM images, as well as optical microscopic images, provided landmark registration for SIMS analysis, where the distributions of both negative ($m/z = 25$) and positive ($m/z = 43$) ions were imaged. Since both CRM and SIMS only imaged a small region of the sample ($150 \mu\text{m} \times 150 \mu\text{m}$), a larger sample area was profiled by LDI-MS, with a spatial resolution of $100 \mu\text{m}$. The LDI-MS image of $m/z = 45$ is shown in Figure 1 as well.

The *Miscanthus* samples in vacuum (SIMS) exhibited no significant structural change when compared to those in air (CRM and optical images). Previous CRM images of *Miscanthus* were acquired in water to reduce unwanted autofluorescence background.³³ However, with improved CRM methodology, the background has been reduced, thereby reducing the need for water immersion. Raman band assignments for *Miscanthus* were given previously.³³ Briefly, the 374 cm^{-1} band is assigned to β -D-glucosides in cellulose; thus, this band was chosen to represent the distribution of cellulose in confocal images. The 1607 and 1630 cm^{-1} bands are assigned to aryl ring vibrations in lignin, and the band at 478 cm^{-1} is characteristic of hemicelluloses. Raman images of *Miscanthus* are clearly dominated by the cell wall, where cellulose and lignin are colocated. Raman bands characteristic of hemicelluloses, another major component of cell walls, are not visible in Figure 1, either because the hemicelluloses in *Miscanthus* cell walls are amorphous and thus exhibit weak Raman response or because their abundance is

-
- (9) Agarwal, U. P. *Planta* **2006**, *224*, 1141–1153.
 - (10) Gierlinger, N.; Schwanninger, M. *Plant Physiol.* **2006**, *140*, 1246–1254.
 - (11) Himmelsbach, D. S.; Khahili, S.; Akin, D. E. *Vib. Spectrosc.* **1999**, *19*, 361–367.
 - (12) Himmelsbach, D. S.; Akin, D. E. *J. Agric. Food Chem.* **1998**, *46*, 991–998.
 - (13) Everall, N. *J. Appl. Spectrosc.* **2000**, *54*, 1515–1520.
 - (14) Everall, N. *J. Appl. Spectrosc.* **2000**, *54*, 773–782.
 - (15) Juang, C. B.; Finzi, L.; Bustamante, C. *J. Rev. Sci. Instrum.* **1988**, *59*, 2399–2408.
 - (16) Belu, A. M.; Graham, D. J.; Castner, D. G. *Biomaterials* **2003**, *24*, 3635–3653.
 - (17) McDonnell, L. A.; Heeren, R. M. A. *Mass Spectrom. Rev.* **2007**, *26*, 606–643.
 - (18) Rubakhin, S. S.; Jurchen, J. C.; Monroe, E. B.; Sweedler, J. V. *Drug Discovery Today* **2005**, *10*, 823–837.
 - (19) Imai, T.; Tanabe, K.; Kato, T.; Fukushima, K. *Planta* **2005**, *221*, 549–556.
 - (20) Andersson, M.; Groseclose, M. R.; Deutch, A. Y.; Caprioli, R. M. *Nat. Methods* **2008**, *5*, 101–108.
 - (21) Debois, D.; Hamze, K.; Guerineau, V.; Caer, J.-P. L.; Holland, I. B.; Lopes, P.; Ouazzani, J.; Seror, S. J.; Brunelle, A.; Laprevote, O. *Proteomics* **2008**, *8*, 3682–3691.
 - (22) Monroe, E. B.; Annangudi, S. P.; Hatcher, N. G.; Gutstein, H. B.; Rubakhin, S. S.; Sweedler, J. V. *Proteomics* **2008**, *8*, 3746–3754.
 - (23) Rubakhin, S. S.; Hatcher, N. G.; Monroe, E. B.; Heien, M. L.; Sweedler, J. V. *Curr. Pharm. Des.* **2007**, *13*, 3325–3334.
 - (24) Burrell, M. M.; Earnshaw, C. J.; Clench, M. R. *J. Exp. Bot.* **2007**, *58*, 757–763.
 - (25) Cha, S.; Song, Z.; Nikolau, B. J.; Yeung, E. S. *Anal. Chem.* **2009**, *81*, 2991–3000.
 - (26) Harada, T.; Yuba-Kubo, A.; Sugiura, Y.; Zaima, N.; Hayasaka, T.; Goto-Inoue, N.; Wakui, M.; Suematsu, M.; Takeshita, K.; Ogawa, K.; Yoshida, Y.; Setou, M. *Anal. Chem.* **2009**, *81*, 9153–9157.
 - (27) Holscher, D.; Shroff, R.; Knop, K.; Gottschaldt, M.; Crecelius, A.; Schneider, B.; Heckel, D. G.; Schubert, U. S.; Svato, A. *Plant J.* **2009**, *60*, 907–918.
 - (28) Metzner, R.; Schneider, H. U.; Breuer, U.; Schroeder, W. H. *Plant Physiol.* **2008**, *147*, 1774–1787.
 - (29) Nemes, P.; Barton, A. A.; Li, Y.; Vertes, A. *Anal. Chem.* **2008**, *80*, 4575–4582.
 - (30) Belu, A.; Mahoney, C.; Wormuth, K. *J. Controlled Release* **2008**, *126*, 111–121.
 - (31) McKeegan, K. D.; Kudryavtsev, A. B.; Schopf, J. W. *Geology* **2007**, *35*, 591–594.
 - (32) Le Naour, F.; Bralet, M.-P.; Debois, D.; Sandt, C.; Guettier, C.; Dumas, P.; Brunelle, A.; Laprévote, O. *PLoS One* **2009**, *4*, e7408.
 - (33) Chu, L.-Q.; Masyukko, R.; Sweedler, J. V.; Bohn, P. W. *Biores. Technol.* **2009**, DOI: 10.1016/j.biortech.2009.10.096.

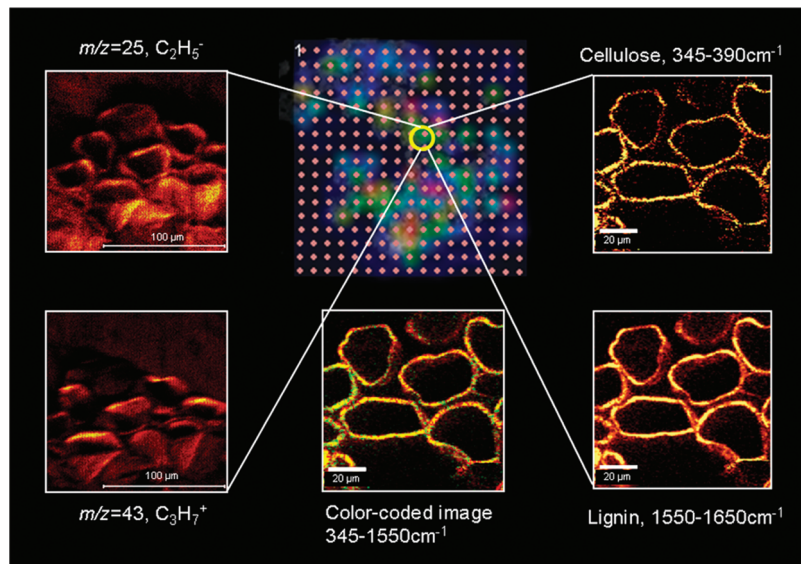


Figure 1. Overview of the LDI-MS/SIMS/CRM spatial correlation strategy. The LDI-MS grid (center top) is color-coded, corresponding to the intensity of $m/z = 45$ ions obtained by laser desorption-ionization excitation spots on $100\text{ }\mu\text{m}$ centers. The yellow circle highlights the spot where high-resolution imaging was performed by both negative ($m/z = 25$, C_2H_5^- , top left) and positive ($m/z = 43$, C_3H_7^+ , bottom left) ion SIMS, as well as CRM, characterized by the cellulose band, $345\text{--}390\text{ cm}^{-1}$ (top right), and the lignin band, $1550\text{--}1650\text{ cm}^{-1}$ (bottom right). (Bottom center) Composite CRM image combining information from both cellulose (green) and lignin (yellow) bands.

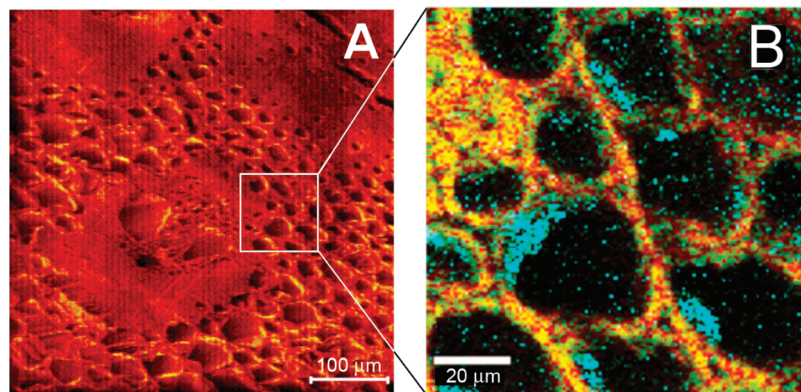


Figure 2. (A) Total negative ion SIMS image of the vascular bundle region. (B) Color-coded CRM image of the boxed ROI in panel A; red = lignin, $1550\text{--}1650\text{ cm}^{-1}$, green = cellulose, $345\text{--}390\text{ cm}^{-1}$, and blue = lignin–hemicellulose complex $460\text{--}500\text{ cm}^{-1}$.

relatively low, so that they are masked by the Raman signal of crystalline cellulose.

In order to elucidate the chemical nature of *Miscanthus*, SIMS experiments were carried out at the identical positions at which the CRM images were acquired. Total secondary ion images (Figure 2A) show a well-preserved cell wall structure. These images also correlate well with the Raman images, indicating that the sample preparation method employed here is well-suited for the analysis of plant samples using SIMS and Raman microscopy. The negative total ion image (Figure 2A) showed better contrast than the positive total image, primarily due to increased secondary ion intensity from hydrogen in the negative mode (Figure S2). The distribution maps of fragment ions corresponding to lignin (m/z 95, $\text{C}_6\text{H}_5\text{OH}_2^+$) and cellulose (m/z 105, $\text{C}_4\text{H}_9\text{O}_3^+$) generally overlap with each other, which is in agreement with the Raman images. The intensity of hemicellulose fragment ions, m/z 133 ($\text{C}_5\text{H}_9\text{O}_4^+$), is weak, making localization of hemicellulose by SIMS difficult (Figure S2 in the Supporting Information).

To overcome the low signal-intensity issue, a region of interest (ROI) analysis of the SIMS data was performed. Figure S3 in the Supporting Information shows the mass spectra obtained from three different ROIs. Spectrum A is the total spectrum, obtained from the accumulation of all secondary ions collected in the total ion image; spectrum B is from the region imaged by CRM, highlighted with a white square in Figure 2A. The spectra from these two regions were essentially identical, indicating that the region imaged with CRM faithfully represents the overall chemical composition of *Miscanthus*. Spectrum C was obtained from an ROI on the interior of the cell. This ROI overlaps with the globular structure highlighted in blue in Figure 2B and is assigned to a hemicellulose-rich lignin complex. A comparison of the mass spectra between the overall structure and the hemicellulose-rich region shows that the intensities of two ions increase significantly: m/z 133 ($\text{C}_5\text{H}_9\text{O}_4^+$), a fragment ion from pentose, and m/z 181 ($\text{C}_6\text{H}_{12}\text{O}_6\text{H}^+$), assigned to either a hexose fragment ion or a pentose cluster ion. Pentose is the scaffold of hemicellulose; therefore, the increased signal intensity of pentose fragment

ions from the globular structure from the interior of the cell confirms the tentative assignment made from the CRM image. Thus, spatially correlated SIMS and Raman imaging provide high-quality, high-resolution subcellular images of *Miscanthus* cross sections, and the combination of information from the mass spectrometry and Raman scattering allows specific chemical assignments of observed structures, difficult to assign from either imaging approach alone.

ACKNOWLEDGMENT

Z.L. and L.-Q.C. contributed equally to this work. We thank Prof. Steven P. Long of the University of Illinois at Urbana–

Champaign for providing *Miscanthus* samples. This project was funded by the Department of Energy through Grant DE FG02 07ER64497.

SUPPORTING INFORMATION AVAILABLE

Additional information as noted in text. This material is available free of charge via the Internet at <http://pubs.acs.org>.

Received for review January 5, 2010. Accepted February 26, 2010.

AC100026R